INVITED PAPER

Benchmarking System-Level Performance of Passive and Active Plasmonic Components: Integrated Circuit Approach

This paper discusses figures of merit for comparing surface plasmon waveguides and introduces several benchmarks for different types of plasmonic modulators.

By Alexey V. Krasavin and Anatoly V. Zayats

ABSTRACT | Using criteria of bandwidth and energy consumption for signal guiding and processing, system-level figures of merit (FOMs) for both passive and active plasmonic circuit components are introduced, benchmarking their performance for the realization of high-bandwidth optical data communication on a chip. The FOM for passive plasmonic interconnects has been derived in terms of the system-level performance of the plasmonic circuitry, emphasising the bandwidth and power dissipation densities. These parameters are linked to the local waveguide characteristics, such as the mode propagation length, bend radius, and mode size. The FOM enables a comparison of the main types of plasmonic waveguides and can serve as a benchmark for future designs of photonic integrated circuits. A FOM for active photonic or plasmonic electro-optical, thermo-optical, and all-optical modulators is also derived to reflect the same benchmarking principles. A particular emphasis is made on establishing a practically oriented benchmark where the integral performance of the circuit, not the size or energy consumption of individual components, plays the defining role.

KEYWORDS | Electro-optical modulators; figure of merit; integrated photonic circuits; nanophotonics; on-chip optical communication; plasmonics

Manuscript received February 17, 2016; revised July 19, 2016; accepted August 10, 2016. Date of publication September 30, 2016; date of current version November 18, 2016. This work was supported by the U.K. Engineering and Physical Sciences Research Council (EPSRC), the Royal Society, and the Wolfson Foundation. All data supporting this research are provided in full in the main text of the manuscript.
The authors are with the Department of Physics, King's College London, London, WC2R 2LS, U.K. (e-mail: alexey.krasavin@kcl.ac.uk).

Digital Object Identifier: 10.1109/JPROC.2016.2603118

I. INTRODUCTION

Microprocessor technology has followed an exponential growth in the computational power for several decades, which is vividly expressed in the empirical Moore's law. The integration level of electronic circuits has already reached the level of ~10 nm. At such dimensions, however, it starts to meet its fundamental limitations. While the operational speed and power consumption of individual metal–oxide–semiconductor field-effect transistors (MOSFETs) improve upon miniaturization, the performance of interconnects linking them follows the opposite trend [1], [2]. With the size reduction, the drastically increased resistance due to the electron scattering on the interconnect boundaries, accompanied by the increase of the lumped capacitance, results in both higher dissipation losses and longer RC delay times. The latter lowers an achievable data exchange rate, while the former leads to parasitic energy consumption.

A new paradigm for interchip and on-chip data traffic can be based on methods already developed for long-haul optical communications [3]–[5], using photonic waveguides with their unprecedented bandwidth. The cross-sectional size of traditional optical waveguides is, however, inherently limited by the diffraction limit of light, which leads to the fundamental mismatch between the integration level of electronic and photonic circuits by almost three orders of magnitude. Implementation of surface plasmon polaritons (SPPs)—electromagnetic waves coupled to free electron oscillations and localized at a dielectric-conductor interface [6]—as signal carriers may provide a solution for eliminating the mismatch [7].

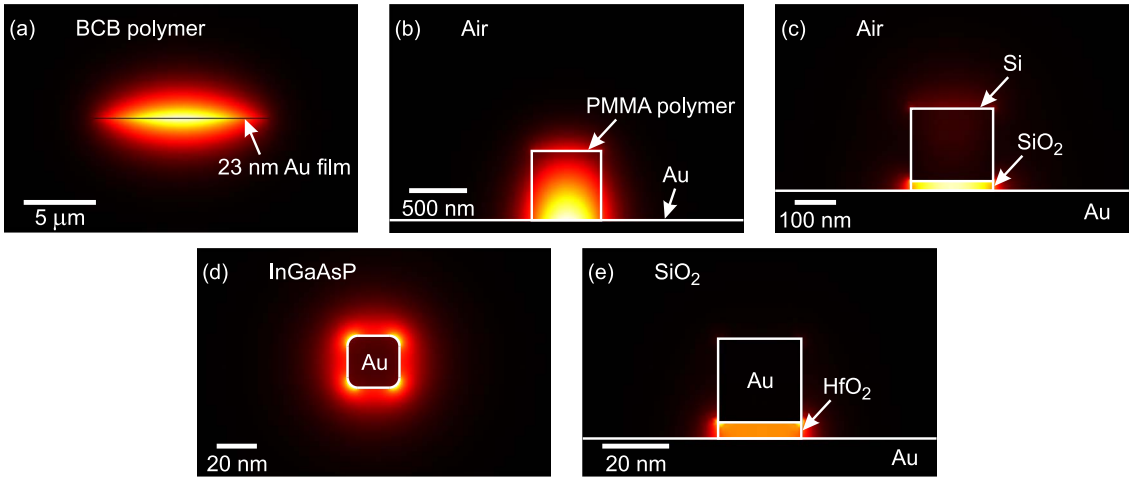

Fig. 1. *Electric field profiles* $|E|^2$ *for the modes in (a) long-range, (b) dielectric-loaded, (c) hybrid, (d) nanowire (asymmetric mode), and (e) wire-MIM plasmonic waveguides. For easy comparison, the results are presented for the same plasmonic platform (Au) and operational wavelength* ($\lambda = 1550$ nm)*. The choice of embedding dielectric (indicated in the figure) is typical for each type of the waveguide.*

Additionally, the plasmonic approach takes advantage of the enhanced light–matter interactions in the vicinity of metallic nanostructures where the field is localized and enhanced, offering a way to create much more compact nanoscale active components for switching, modulating, and conditioning of optical signals using nanoscale electro-optical and nonlinear optical phenomena [8]–[10], and furthermore bringing ultrafast operation speeds [11], [12] and ultralow energy consumption. Plasmonic components, however, introduce significant propagation and insertion losses in photonic circuitry. The important question is, therefore, whether the advantages in the circuit miniaturization, speed increase, and the reduction of energy consumption provided by the plasmonic approach outweigh the penalty of the energy dissipation in individual plasmonic active and passive components when considering the photonic system as a whole.

In this paper, we address this question by deriving, from the bandwidth and energy consumption considerations of the integrated photonic system, benchmarking parameters [figures of merit (FOMs)] characterizing the performance of 1) plasmonic waveguides for the on-chip data communication; and 2) active plasmonic components, particularly, modulators. Importantly, for the passive components, the FOM was obtained on the basis of most general and practically relevant considerations of the data traffic rate and power dissipation densities, which appeared to be related to the widely used local waveguide characteristics, such as the bandwidth, signal propagation length, and integration parameters. This allows the generalization of all earlier FOM considerations and reveals a previously overlooked bandwidth factor. On this basis, the performance of the main types of plasmonic waveguides is benchmarked. In the second part of the paper, a FOM for optical modulators is derived. Taking advantage of the localization of optical signals at the nanoscale dimensions, plasmonic electro-optical and all-optical modulators have extremely small sizes, which leads to their extremely high operational speeds (possibly tens of terabits per second) and low energy consumption (below a femtojoule per bit). The FOM of plasmonic modulators reveals their qualitative advantages compared to the best traditional state-of-the-art photonic counterparts.

II. FOM FOR PASSIVE PLASMONIC WAVEGUIDES

Considering the advantages offered by the plasmonic approach in the size reduction of nanophotonic components, a broad variety of plasmonic waveguiding geometries has been proposed, including long-range [13], [14], dielectric-loaded [15], hybrid [16], [17], nanowire [18], metal–insulator–metal (MIM), and wire-MIM [8] plasmonic waveguides, to name just a few (Fig. 1). These designs cover the whole range of guided mode sizes achievable in the optical communication wavelength range from micrometers, as in long-range plasmonic waveguides [Fig. 1(a)], to tens of nanometres as, e.g., in wire and wire-MIM plasmonic waveguides [Fig. 1(d) and (e)]. For all these waveguides, however, the achieved signal localization is accompanied by intrinsic Ohmic losses introduced by the metallic elements of the waveguides, resulting in a propagation loss of the plasmonic signal. The propagation length of the signal L_{prop} (after which the mode intensity decreases e times), therefore, ranges from a centimeter scale (as in long-range plasmonic waveguides) for the waveguides with lower signal

localization to a micrometer scale for the waveguides with the highest confinement, e.g., in wire and wire-MIM plasmonic waveguides. In fact, there is a general tradeoff between these two characteristics: higher mode localization usually corresponds to a larger relative part of the mode energy propagating in the metal, which leads to higher losses and, therefore, a lower propagation length.

In order to compare the diverse variety of plasmonic waveguides, a FOM can be introduced to quantitatively characterize their guiding performance. The first FOM to characterize the performance of various passive waveguides was introduced by Buckley and Berini [19]. As the best starting point, the FOM

$$M_1 = 2\sqrt{\pi} \cdot \frac{L_{\text{prop}}}{\sqrt{S}} \tag{1}$$

represented a straightforward measure of the aforementioned tradeoff: a ratio between the signal propagation length L_{prop}, reflecting the propagation characteristic of the mode and the size of the mode $\sqrt{S}$ (with S being the effective mode area), reflecting the mode confinement. Although it has a clear physical meaning and gives a vivid characterization of the mode as such, this FOM is not ideal for benchmarking the performance of the waveguides implemented in highly integrated optical circuits. The square root of the mode area in the denominator of M_1 is effectively a measure of how closely parallel waveguides can be placed on a chip. However, modes with the same effective areas can couple with different efficiency to a neighboring waveguide depending on their spatial field distributions. Furthermore, it was shown that there is a variety of ways to quantify the effective mode area, frequently giving essentially different and even opposite results (for an extensive overview, see [20]).

In the further development, the FOM was modified in order to include a direct measure of the coupling efficiency [18], [21]. When two parallel waveguides are placed next to each other, their coupling leads to a gradual transfer of the mode from one waveguide to another with full energy relocation after a distance L_{coupl}. Taking this into account, the waveguide center-to-center separation d_{sep} representing how close the two identical waveguides can be placed, so that the coupling distance $L_{\text{coupl}}(d_{\text{sep}}) = 4L_{\text{prop}}$, will give a direct measure of the achievable integration density: after one propagation length, only 15% of the mode energy will be coupled to the neighboring "aggressor" waveguide. Such a condition, expressing the coupling length in terms of the propagation length, was chosen to compare diverse guiding approaches, embracing an extremely wide range in the propagation-confinement parameter space. (Here we note that although this definition is universal, it is postulated leaving the degree of freedom for adjusting it to a particular application, for example, instead of L_{prop}, a characteristic interconnect length L_{int} can be used if $L_{\text{prop}} > L_{\text{int}}$.) Using the coupling distance considerations, the FOM can be represented as [21]

$$M_{\text{loc}}^{\text{lin}} = \frac{L_{\text{prop}}}{d_{\text{sep}}}. \tag{2}$$

Notably, although the coupling phenomenon involves mode evolution in the third dimension along the waveguides, seemingly requiring 3-D numerical simulations, the coupling characteristic $(L_{\text{coupl}}(d_{\text{sep}}))$ can be derived from a 2-D eigenmode analysis of two coupled waveguides [21]. Particularly, this can be done by monitoring the difference between mode effective indexes of the symmetric $(n_{\text{eff}}^{\text{sym}})$ and antisymmetric $(n_{\text{eff}}^{\text{asym}})$ modes appearing in such a system $L_{\text{coupl}} = \lambda/[2(n_{\text{eff}}^{\text{sym}} - n_{\text{eff}}^{\text{asym}})]$, where λ is the operational wavelength. Therefore, it has the same numerical simulation complexity as the usual modal area estimation.

The second main parameter characterizing particularly the performance of a multibranched waveguide circuitry is an optimal bend radius, minimizing signal loss along a curved waveguide section. This parameter defines the size of all circuit components, such as splitters, waveguide ring resonators (WRRs), Mach–Zehnder interferometers (MZIs), etc. The optimal waveguide radius is a tradeoff between Ohmic loss (higher for bigger radii) and radiation losses (higher for smaller radii) [22], [23]. A FOM $M_2 = 2L_{\text{prop}} \cdot (n_{\text{eff}} - n_{\text{surr}})$ [19], where n_{eff} is the mode effective index and n_{surr} is the refractive index of the surrounding medium, gives only a partial answer, introducing an approximate measure of only the radiation losses: the further the SPP mode dispersion is from the light line, the lower is the coupling efficiency to the escaping light. At the same time, the radiation losses are also influenced by the particular waveguide geometry, and can be different for waveguides with the same value of the FOM M_2. As an alternative approach, the FOM for multibranched plasmonic circuitry was proposed in [18], taking into account both Ohmic and radiation losses and directly estimating the waveguide bends performance

$$M_{\text{loc}} = \frac{L_{\text{prop}}}{d_{\text{sep}}} \cdot \left(\frac{T(r)}{r}\right)_{\max} \tag{3}$$

where $(T(r)/r)_{\max}$ is the maximum value of the ratio of the transmission $T(r)$ and bend radius r, which can be found varying the radius in 3-D numerical simulations.

The above FOMs were derived using local characteristics of the waveguide performance: the propagation

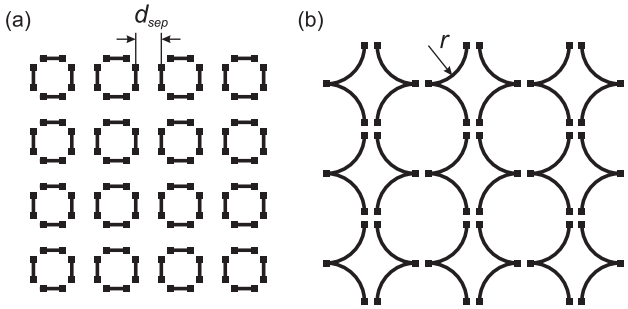

Fig. 2. *Two extreme scenarios for data network layout: (a) the network consists of only straight waveguides and (b) the network consists of only circularly curved waveguides relevant to waveguide bends, splitters, and ring resonators (in the case of waveguide bends and splitters, one can get approximately 10% improvement in performance using harmonic-function-based shapes [15], [23]). The minimum curvature radius r with still affordable radiation losses is usually bigger than the separation distance d_{sep} with the affordable crosstalk.*

length, crosstalk between neighboring waveguides, and bent waveguide performance. The most relevant to practical applications, however, is the estimation of the system-level performance of the multibranched plasmonic circuit, when considered as a complete data communication architecture. The most general benchmark describing the performance from this point of view can be defined considering the bandwidth and energy requirements for transferring a signal

$$M_{\text{syst}} = \frac{b}{p} \tag{4}$$

where b is the bandwidth density which is a number of bits transferred per second per unit area of an integrated circuit [24] and p is the power density required to sustain the bitrate (in the case of plasmonic waveguides this is the power lost in transmission due both radiation and absorption losses). To estimate such a FOM related to system-level performance, we consider two extreme scenarios for the network layout (Fig. 2).

In the first case, the circuit consists solely of straight waveguides, connecting input and output nodes. We will consider the most dense layout where the distance between the nodes is the smallest and equal to the separation distance between two parallel waveguides d_{sep} [Fig. 2(a)]. Using the smallest unit cell $2d_{\text{sep}} \times 2d_{\text{sep}}$, the highest bandwidth density with straight interconnects achievable for each type of the waveguides can be estimated $b = B/d_{\text{sep}}^2$, where B is the highest bandwidth (i.e., the highest bitrate which can be transmitted by a waveguide of a given length). It should be noted that a bitrate and, therefore, a bandwidth density can be increased using, e.g., wavelength division multiplexing (WDM) by transmitting several bitstreams through the same waveguide simultaneously at different carrier wavelengths, or other techniques. The total bandwidth is then $B = NB_1$, where N is the number of channels, considered to be equal for all plasmonic waveguides and B_1 is the bandwidth of a single data stream. The bandwidth B_1 is limited for a single-mode waveguide by the group velocity dispersion (GVD) and nonlinear effects which differently affect the propagation conditions for different spectral components of the signal, leading to its distortion. In lossy waveguides, broadening of the pulses depends on the second-order dispersion of both real and imaginary parts of the propagation constant β [25]

$$B_1 \sim L^{-1/2}\left(\left(\frac{\partial^2 \text{Re}\{\beta\}}{\partial\omega^2}\right)^2 + \left(\frac{\partial^2 \text{Im}\{\beta\}}{\partial\omega^2}\right)^2\right)^{-1/4}. \tag{5}$$

For the plasmonic waveguides compared below, it was found that $(\partial^2 \text{Im}\{\beta\}/\partial\omega^2)^2 \ll (\partial^2 \text{Re}\{\beta\}/\partial\omega^2)^2$, which is determined by both the material and modal dispersions. Since $\partial^2 \text{Im}\{\beta\}/\partial\omega^2$ is one or two orders of magnitude smaller than $\partial^2 \text{Re}\{\beta\}/\partial\omega^2$, depending on the waveguide type, and leads to the correction to the bandwidth less than 0.3%, it can be neglected, and the bandwidth can be estimated as [26]

$$B_1 = \left(8\pi L \frac{\partial^2 \text{Re}\{\beta\}}{\partial\omega^2}\right)^{-1/2} = \left(8\pi \frac{L}{v_g^2}\frac{\partial v_g}{\partial\omega}\right)^{-1/2} \tag{6}$$

where v_g is the group velocity of the mode and L is the interconnect length. For the estimation of the bandwidth, the length of the plasmonic interconnect was taken to be equal to the propagation length $L = L_{\text{prop}}$. It should be noted, from the discussion related to (5) and (6), that for the description of pulse propagation in the considered cases it is possible to apply the concept of the group velocity, otherwise the approach based on the energy velocity should be used. The nonlinear effects (affecting the bandwidth in the case of optical fibers) were not taken into account because, for small interconnect lengths and low targeted pulse energy of approximately 1 fJ [27], [28], these effects are small even considering the larger nonlinearity in gold and the field enhancement in the plasmonic mode.

Considering the same average power p_0 sent through each interconnect, the power loss per unit area can be estimated as

$$p = p_0\left(1 - \exp[-d_{\text{sep}}/L_{\text{prop}}]\right)/d_{\text{sep}}^2 \approx p_0/(d_{\text{sep}}L_{\text{prop}}) \tag{7}$$

where the fact that $d_{sep} \ll L_{prop}$ was taken into account. This results in the following system-level FOM for the integrated circuit in Fig. 2(a):

$$M_{syst}^{lin} = \frac{b}{p} \sim B_1 \frac{L_{prop}}{d_{sep}}. \quad (8)$$

In the second case [Fig. 2(b)], if the circuitry is predominantly multibranched, both the bandwidth density and the power loss will be primarily defined by the performance of the waveguide bend. Here, as a universal building shape for waveguide bends, splitters, and ring resonators, a bend shape is considered in a form of a circular arc. In this case, the bandwidth per unit area is equal to $b = B/r^2$, while the corresponding loss density is equal to $p = (1 - \exp[-1/4 \cdot 2\pi r/L_{prop}^{bend}(r)])/r^2$, where r is the bend radius and $L_{prop}^{bend}(r)$ is the propagation length of the mode along the bend, determined by both Ohmic and radiative losses. Taking into account that the transmission through a bend is usually reasonably high (~0.75–0.95), and, thus, $1/4 \cdot 2\pi r/L_{prop}^{bend}(r) \ll 1$, we can approximate $p \approx 1/2 \cdot \pi L_{prop}^{bend}(r)/r$. The FOM for such circuit is then given by

$$M_{syst}^{circ} = \frac{b}{p} \sim B_1 \left(\frac{L_{prop}^{bend}(r)}{r} \right)_{max} \quad (9)$$

where $(L_{prop}^{bend}(r)/r)_{max}$ is the highest value of the ratio of the propagation length along the bend and its radius for a given waveguide type. Finally, in the case of an arbitrary circuitry layout, we can combine these two FOMs and obtain

$$M_{syst} = B_1 \cdot \frac{L_{prop}}{d_{sep}} \cdot \left(\frac{L_{prop}^{bend}(r)}{r} \right)_{max}. \quad (10)$$

Strikingly, although the local [see (3)] and system-level FOMs are derived from absolutely different perspectives, they reflect absolutely the same dependences on the waveguide performance characteristics. The only difference is that in the former case the bend transmission-to-radius ratio $T(r)/r$ is maximized, while in the latter case, the same should be done for the propagation characteristic of the bend section $L_{prop}^{bend}(r)/r$. It should be noted that the transmission through the bend $T(r)$ and the propagation length along the bend $L_{prop}^{bend}(r)$ are closely related characteristics. Another important parameter in (10), which was completely disregarded previously, is the waveguide bandwidth, which is revealed using the system-level performance approach. Due to small interconnect lengths, the calculated single-stream bandwidth B_1 reaches extremely high values of tens of terabits per second (Table 1), and practically will be limited by available data modulation and detection electronic technologies presently capable of 10–100-Gb/s modulation rates.

The derived system-level FOM was evaluated to compare the performance of the main types of plasmonic waveguides (Table 1). The relevant waveguide characteristics were found using 2-D eigenmode and full 3-D finite element numerical simulations. For fair comparison, all the waveguides were implemented on a gold material platform at telecommunication wavelength $\lambda = 1550$ nm. Additionally, for the wire-MIM waveguide, an Al platform was used to compare the performance of the original design [8] and for the wire waveguides, two different dielectric coatings were implemented. The optical constants of metals were taken from [29]. As expected, for all the waveguides, a tradeoff between L_{prop} and d_{sep} is observed (Table 1). The propagation length along the optimally curved section L_{tot} is a factor of 1.2–4 shorter than L_{prop} as it also includes the radiation losses. The ideal radius can be of the same order of magnitude as the waveguide cross sections, as in the case of the most highly integrated waveguides, or can be up to three orders of magnitude larger, as in the case of the long-range SPP waveguides. There is a clear trend of the increase of the waveguide bandwidth for the waveguides allowing a higher integration level, which can be partly explained by a shorter distance along which the pulse needs to propagate (L_{prop}) and thus GVD has less influence.

An interesting universal tendency encompassing the characteristics of plasmonic waveguides of completely different designs can be observed. For instance, the crosstalk limited photonic integration density of straight waveguides can be different by two orders of magnitude, the bend radii can be different by five orders of magnitude, propagation lengths can be different by four orders of magnitude (cf., d_{sep}, r, and other parameters for long-range and wire-MIM SPP waveguides), but the system-level FOMs for all waveguide types fall within two orders of magnitude interval. As follows from Table 1, for particular parameters of plasmonic waveguide designs taken from the literature, the hybrid plasmonic waveguides have the highest FOM values; however, one needs to bear in mind that the FOM for a given waveguide design may vary with its geometrical parameters (e.g., for hybrid waveguides, the FOM can vary by an order of magnitude for different parameters). In this regard, apart from benchmarking the performance of waveguides of various designs, the derived FOM can be used to optimize the performance of a chosen type of the waveguide. For complete assessment, the FOM should be used in conjunction with other technological considerations, such as compatibility of the waveguides' material platform with the existing fabrication processes or the cost of mass production of such circuits, and, in particular, with the specific application requirements, which may prioritize one or another performance characteristic of a waveguide interconnect.

Table 1 Benchmarking Characteristics of Various Optical Waveguides and Comparison of their Performance using the System-Level FOM (10)

	Long-range waveguide [13]*	DLSPPW [15]	Hybrid waveguide	Wire waveguide (asym. mode) [18]	Wire-MIM waveguide [8]	250 nm × 400 nm SOI waveguide
B_1	14 Tb/s	39 Tb/s	70 Tb/s** ([16]) 20 Tb/s ([17])	61 Tb/s (InGaAs coat.) 90 Tb/s (SiO_2 coat.)	139 Tb/s (Al) 86 Tb/s (Au)	3.2 Tb/s
L_{prop}	1.75 mm	45 μm	45 μm ([16]) 16.3 μm ([17])	310 nm (InGaAs coat.) 1.2 μm (SiO_2 coat.)	420 nm (Al) 480 nm (Au)	~1 cm (limited by waveguide wall roughness)
d_{sep}	12 μm	1.8 μm	1.05 μm ([16]) 1.3 μm ([17])	85 nm (InGaAs coat.) 200 nm (SiO_2 coat.)	65 nm (Al) 60 nm (Au)	1.2 μm
L_{prop}^{bend}	1.1 mm	31.5 μm	38 μm ([16]) 15.1 μm ([17])	110 nm (InGaAs coat.) 123 nm (SiO_2 coat.)	196 nm(Al) 405 nm (Au)	350 μm
r	3 mm	6 μm	2 μm ([16]) 3.5 μm ([17])	12.5 nm (InGaAs coat.) 12.5 nm (SiO_2 coat.)	12.5 nm (Al) 12.5 nm (Au)	2.9 μm
M_{syst}	$0.75\cdot10^3$ Tb/s	$6.1\cdot10^3$ Tb/s	$56.9\cdot10^3$ Tb/s ([16]) $1.1\cdot10^3$ Tb/s ([17])	$2\cdot10^3$ Tb/s (InGaAs coat.) $5.3\cdot10^3$ Tb/s (SiO_2 coat.)	$14.1\cdot10^3$ Tb/s (Al) $22.3\cdot10^3$ Tb/s (Au)	$3.2\cdot10^6$ Tb/s

*Although assumption $1/4\cdot 2\pi r/L_{prop}^{bend}(r) \ll 1$ is not valid for long-range SPP waveguides, the calculated figure of merit can be treated as an upper estimate.
**In all the considered cases, the variation of the group velocity dispersion over the waveguide bandwidth is below 5%, except for the hybrid waveguide from Ref. [16] with about 10% variation due to the higher-order effects (this would affect a FOM by not more than ~10%).

[A typical example of these may be given considering, e.g., conventional silicon-on-insulator waveguides with a very low propagation loss which would provide very high FOM (Table 1) but their applications are limited to low integration densities of global optical interconnects.]

It also needs to be noted that the insertion losses of nanophotonic circuitries in, e.g., fiber-based networks play an important role for determining the power efficiency of the chosen photonic integrated circuit architecture, but they are similar for all the waveguides considered. Moreover, for fully integrated applications, on-chip nanoscale light sources for generating light and/or SPPs directly into the plasmonic waveguided modes under either electrical [30], [31], or optical [32] excitation can be implemented.

III. FOM FOR ACTIVE PLASMONIC COMPONENTS

The advantages which the plasmonic approach brings to the development of electro-optical, thermo-optical, or all-optical modulators and switches are related to their small size and increased light–matter interaction strength near plasmonic interfaces [8], [33]–[36], thus reducing the required operational energy and increasing speed. To achieve quantitate comparison of various optical modulators, an "active" FOM is needed which takes into account all application requirements.

The performance of optical modulators is mainly characterized by two parameters: the achievable modulation speed (or modulation bandwidth) and the energy consumption per bit [33]. In the case of electro-optical modulation, the modulation bandwidth is defined by the *RC*-delay of the component:

$$B_{\mathrm{mod}} = \frac{1}{\tau} = \frac{1}{RC} \tag{11}$$

where R is the external resistive load, taken to be the same (500 Ohm) for all the bandwidth estimations below, and C is the capacitance of the device (determined

by the electrical contact through which the control voltage is applied to the device), which is directly proportional to the characteristic device size a. The simplest example is a parallel plate capacitor, for which the area $S \sim a^2$ and the gap between plates $d \sim a$, and, therefore, the capacitance $C = \varepsilon_0 \varepsilon S/d \sim a$ (here, ε_0 and ε are the permittivities of vacuum and the material between plates, respectively). This explicitly shows the advantage of nanoscale sizes of plasmonic modulators for the increase of the modulation speed.

The energy consumption per bit can be estimated as the energy required to charge the effective device capacitor to the required voltage $V_{3\text{-dB}}$ returning 3-dB intensity modulation through the induced change of the mode phase or absorption [37]

$$P = \frac{1}{4} C V_{3\text{-dB}}^2. \tag{12}$$

Since the control voltages of the plasmonic modulators are of the same order of magnitude as for their conventional photonic counterparts [8], [33]–[36], [38], [39], a requirement $P \sim C \sim a$ underlines a crucial advantage offered by the plasmonic approach: reducing the modulator size leads to the reduced energy consumption.

In addition to the above main characteristics, other important operational parameters should be considered such as contrast ratio, optical bandwidth (the wavelength range in which the modulator can operate, which also affects the modulation speed), insertion loss, footprint, and the optical power it can accommodate. As a consequence, a huge variety of FOMs benchmarking the performance of optical modulators exists considering different characteristics to be the most important ones and relevant to different modulator designs. At the same time, a universal modulator FOM capable of comparing various designs and approaches from a point of view of system-level performance is absent.

A good starting point for the development of such a FOM is the most common benchmark, used for conventional phase-shift electro-optical modulators based on Mach–Zehnder interferometers [40]

$$M_1^{\text{act}} = \frac{1}{V_{3\text{-dB}} l} \tag{13}$$

where l is the modulator length. This FOM can also be applied to absorption-based modulators, while a FOM of the same form $M_1^{\text{act}} = 1/(V_{3\text{-dB}} r)$ can be introduced for another common phase-shift design based on a ring resonator, where r is the ring radius characterizing the device optical path. An advantage of M_1^{act} is that it brings to the focus the efficiency of modulation *design* and the performance of the *materials* rather than the overall device performance. It, however, completely disregards such an important parameter as the switching speed (modulation bandwidth B_{mod}). As an alternative, another FOM has been proposed [41]

$$M_2^{\text{act}} = \frac{B_{\text{mod}}}{V_{3\text{-dB}}}. \tag{14}$$

Using (11), one can rewrite it as

$$M_2^{\text{act}} = \frac{1}{V_{3\text{-dB}} RC} \sim \frac{1}{V_{3\text{-dB}} Rl} \sim M_1^{\text{act}} \tag{15}$$

and conclude that for the case of a fixed waveguide cross section, it is analogous to M_1^{act}.

The difficulties arise when one tries to apply these FOMs to assess the practical performance of the component when integrated in circuitry and uses the energy consumption as the modulator characteristic. For example, between the two modulators of the same cross section having the same values of M_1^{act}, the one which has twice smaller l (and, therefore, twice larger $V_{3\text{-dB}}$) will have a power consumption of two times higher, as it follows from (12). Therefore, considering the practical performance of the modulator as an integral part of a chip, one logically comes to a widely used FOM based on the electrical power required for component switching, rather than voltage [42]

$$M_3^{\text{act}} = \frac{B_{\text{mod}}}{P}. \tag{16}$$

Finally, including in the FOM a factor which became particularly important with the development of the plasmonic-based modulators—modulator ON-state attenuation due to the increased optical losses [43], expressed through transmission coefficient A in the ON-state—we arrive to the final expression for the modulator FOM on the basis of the system-level performance

$$M_4^{\text{act}} = A \frac{B_{\text{mod}}}{P}. \tag{17}$$

Using (11) and (12), it can be simplified to $M_4^{\text{act}} = 4A\left(RV_{3\text{ dB}}^2 C^2\right)^{-1} \sim a^{-2}$. This immediately confirms the advantages of plasmonic electro-optic modulators, having the potential for extremely small sizes a. This further illustrated by benchmarking various designs (Table 2). It is also worth noting that due to the universal character of the parameters in M_4^{act}, it can also be applied for other types of optical modulators, e.g., all-optical, thermo-optical, or opto-mechanical.

Table 2 Benchmarking Characteristics of Various Modulators and Comparison of their Performance using FOM (17)

	Commercial $LiNbO_3$ modulator	Si ring resonator modulator [38]	GeSi electro-absorption modulator [39]	Electro-optical plasmonic modulator [34]	Field-effect plasmonic modulator	Plasmonic all-optical modulator [9]	Si-photonics nonlinear demultiplexer [44]	Metama-terial-based all-optical modulator [45]
B_{mod}	40 Gb/s	10 Gb/s	40 Gb/s	400 Gb/s	500 Gb/s (10 Tb/s) ([35])** 15 Tb/s ([8])	15 Gb/s	1 Tb/s	0.1—1 Tb/s
P	10 pJ	50 fJ	60 fJ	60 fJ	4 fJ (30 aJ) ([35]) 15 aJ ([8])	0.3 fJ	1 pJ	3.7 pJ
S	5 cm^2	1000 μm^2	500 μm^2	30 μm^2	1 μm^2 ([35]) 10^{-2} μm^2 ([8])	300 μm^2	1 $\mu m \times 4$ mm	0.5 μm^2
A	0.3*	0.6	0.3	0.1	0.8 ([35]) 0.6 ([8])	0.1	1	0.3
B_{opt}	40 nm	0.1 nm	35 nm	>100 nm	≫100 nm	≫100 nm	n/a	20 nm
M_4^{act}	~0.001 Gb/s/fJ	0.12 Gb/s/fJ	0.2 Gb/s/fJ	0.7 Gb/s/fJ	50 Gb/s/fJ ($3 \cdot 10^5$ Gb/s/fJ) ([35]) $6 \cdot 10^5$ Gb/s/fJ ([8])	5 Gb/s/fJ	1 Gb/s/fJ	0.01-0.1 Gb/s/fJ

* The value of $A = 0.3$ corresponds to 30% modulator transmission in the on-state.

** Table values for the modulator Ref. [35]: without brackets – conservative estimation from the original article [35] for a load of 500 Ohm: in brackets – potential value for an optimised design.

If one divides both the numerator and the denominator of (17) by the modulator footprint S:

$$M_4^{\text{act}} = A\frac{B_{\text{mod}}/S}{P/S} = A\frac{b_{\text{mod}}}{p} \tag{18}$$

one can see another meaning of the FOM: it presents a balance between the active bandwidth density b_{mod} and the power density p required to achieve it. In other words, the FOM remains the same if the increased integration density of the switching components is balanced by a proportional increase in switching energy consumption of a circuit as a whole. If, however, the integration level is a major consideration so that the components with smaller footprint become preferable, the higher rate of increase of the circuit energy consumption should be allowed for.

The impact of the optical bandwidth B_{opt} on the performance of the optical modulator is more difficult to account for, as it has a technological character (fabrication precision, temperature stability, etc.), therefore, this parameter was not included in the FOM. Apart from this, in highly resonant systems, such as ring resonators or photonic crystal cavities, the low optical bandwidth (corresponding to a long resonance buildup time) decreases the modulation bandwidth B_{mod}, which competes with the bandwidth defined by the *RC*-delay, and can become the major factor limiting the overall bandwidth value.

Several observations can be made from the data in Table 2 comparing various modulator designs. Two mainstream electro-optic designs (columns 3 and 4) which are under consideration to replace the commercial $LiNbO_3$ modulators (column 2), namely, Si ring-resonator modulators, based on a free carrier dispersion effect, and GeSi modulators based on an electro-absorption effect do offer better performance in the system-level settings. These three types of modulators have comparable modulation bandwidths and most of the other parameters, but smaller size and, consequently capacitance, of the Si- and GeSi-based designs ensures lower energy consumption characteristics, which are on fJ rather than pJ scale. Such a performance improvement is reflected in a straightforward way in the hundred-fold increase of the FOM (here, one needs to consider that the optical bandwidth of the Si-based modulator is rather narrow due to the use of a highly resonant system). Another several times increase in the FOM can be achieved implementing plasmonic approach, which provides further reduction of the device size, combining it with an efficient active material platform (a polymer with electro-optical Pockels effect, column 5). The main role in the FOM improvement is played here by

an order of magnitude higher modulation bandwidth, while the energy consumption remained at the same level due to a rather high (5–7.5 V) modulation voltage and additional price for the plasmonic design is paid in a form of absorption losses (cf. column 5 and columns 3 and 4). In the examples of field-effect plasmonic modulators (column 6), the nanoscale dimensions of the device and, particularly, the extreme localization of plasmonic modes was combined with strong electro-absorption effect, capable to act on the modes at the nanoscale. Thus, the obtained very-low-capacitance devices provide both high (terabits per second range) modulation bandwidth and femtojoule (potentially attojoules) power consumption per bit; all these parameters result in the highest FOM among the considered electro-optical modulators.

To demonstrate the universal character of the derived FOM, several examples of all-optical modulators were considered (columns 7–9). Here, due to variety of available designs and material platforms, the operational characteristics span wide range of parameters: modulation bandwidth varies from gigabits per second to terabits per second, power consumption from subfemtojoule to a few picojoules, with up to two orders of magnitude difference in sizes. Generally, the presented FOMs are comparable to that of the considered electro-optic modulators, but in our view they should be benchmarked within their own all-optical domain, since they present a completely different all-optical chip paradigm than electro-optical devices. In the future, all-optical modulators have a potential of achieving the highest FOMs due to very high modulation rates available with third-order nonlinear processes [44], [46], [47].

Finally, to complete the overview of available and future switching and modulation technologies, thermo-optical and nano-opto-mechanical approaches should be mentioned. Thermo-optical switches are low-speed (kilohertz–megahertz range) devices in both photonic [48] and plasmonic [49] realizations, important for some applications in signal routing and variable-optical attenuators. Potentially, plasmonic-based devices of this type should provide better FOMs than dielectric photonic ones due to smaller sizes and, thus, reduced power consumption. However, their fair comparison was not possible with the available published data due to very different thermo-optical materials used. Nanomechanical approaches for photonic modulators and switches may provide some of the lowest switching energies per bit with moderate megahertz-range speeds in both photonic and plasmonic environments [50]–[53].

IV. CONCLUSION

FOMs for passive plasmonic interconnects and active components (modulators) were derived on the basis of system design requirements and the most general considerations describing their efficiency to realize high-bandwidth data communication in multibranch photonic circuitry. Particularly, for the passive waveguide components, a ratio of a bandwidth density to the corresponding power dissipation was chosen as an ultimate practical characteristic benchmarking their performance. Such a FOM was further expressed in terms of standard local waveguide characteristics, such as signal propagation lengths along straight and curved waveguide sections, crosstalk distance, and an optimal bend radius. Interestingly, it provided a general validation of the "local" FOMs but making different accents on which particular parameters characterizing waveguide performance are important (e.g., transmission coefficient versus propagation length along a curved section). The obtained FOM provided an insightful comparison of the performance of the main types of nanophotonic waveguides and showed the ability to efficiently benchmark circuitries on the basis of waveguides with hugely diverse range of characteristics as well as to optimize particular designs.

Furthermore, the advantages of the plasmonic approach for the development of active components for on-chip data-transfer photonic circuits have been clearly identified. In particular, plasmonic electro-optical modulators needed to establish communication between electronic and optical signals at the nanoscale have been discussed. The key features of plasmonic modulators have been elucidated, namely, their extremely small size which leads to the simultaneous improvement of two key modulator characteristics: the increase of the operational speed and the decrease of the energy consumption per bit. This was demonstrated through derivation of a FOM for optical modulators and benchmarking various photonic and plasmonic designs and approaches. Thus, from the perspective of both passive and active functionalities, the plasmonic approach paves the way for the development of highly efficient hybrid electronic/photonic chips where the information will be processed electronically, but transferred optically. Even now, it can essentially increase the bandwidth of current data communication, despite the increased insertion and propagation losses that are counteracted by the system-level improvement in terms of overall required energy and performance. Potential use of new plasmonic materials [54] may further help with reduction of size and energy consumption in nanophotonic integrated circuits and thus bring improvements of the system-level FOM, additionally extending range of CMOS-compatible designs. Further developments in finding new active materials and optimizing the effects for improved electro-optical, thermo-optical, and all-optical modulation will benefit both plasmonic and conventional photonic modulators. ■

REFERENCES

[1] D. A. B. Miller, "Rationale and challenges for optical interconnects to electronic chips," *Proc. IEEE*, vol. 88, no. 6, pp. 728–749, 2000.

[2] C. Sun *et al.*, "Single-chip microprocessor that communicates directly using light," *Nature*, vol. 528, pp. 534–538, 2015.

[3] M. J. Kobrinsky *et al.*, "On-chip optical interconnects," *Intel Tech. J.*, vol. 8, no. 2, pp. 129–141, 2004.

[4] P. M. Watts, S. W. Moore, and A. W. Moore, "Energy implications of photonic networks with speculative transmission," *J. Opt. Commun. Netw.*, vol. 4, no. 6, pp. 503–513, 2012.

[5] S. Liu *et al.*, "Low latency optical switch for high performance computing with minimized processor energy load," *J. Opt. Commun. Netw.*, vol. 7, no. 3, pp. A498–A510, 2015.

[6] A. V. Zayats, I. I. Smolyaninov, and A. A. Maradudin, "Nano-optics of surface plasmon polaritons," *Phys. Rep.*, vol. 408, no. 3–4, pp. 131–314, 2005.

[7] J. Takahara and T. Kobayashi, "From subwavelength optics to nano-optics," *Opt. Photon. News*, 54–59, Oct. 2004.

[8] A. V. Krasavin and A. V. Zayats, "Photonic signal processing on electronic scales: Electro-optical field-effect nanoplasmonic modulator," *Phys. Rev. Lett.*, vol. 109, 2012, Art. no. 053901.

[9] K. F. MacDonald and N. I. Zheludev, "Active plasmonics: Current status," *Laser Photon. Rev.*, vol. 4, no. 4, pp. 562–567, 2000.

[10] C. Haffner *et al.*, "All-plasmonic Mach–Zehnder modulator enabling optical high-speed communication at the microscale," *Nature Photon.*, vol. 9, pp. 525–528, 2015.

[11] M. I. Stockman, "Nanoplasmonics: Past, present, and glimpse into future," *Opt. Exp.*, vol. 19, no. 22, pp. 22029–22106, 2011.

[12] K. F. MacDonald, Z. L. Sámson, M. I. Stockman, and N. I. Zheludev, "Ultrafast active plasmonics," *Nature Photon.*, vol. 3, pp. 55–58, 2009.

[13] A. Degiron *et al.*, "Experimental comparison between conventional and hybrid long-range surface plasmon waveguide bends," *Phys. Rev. A*, vol. 77, 2008, Art. no. 021804(R).

[14] A. V. Krasavin and A. V. Zayats, "Numerical analysis of long-range surface plasmon polariton modes in nanoscale plasmonic waveguides," *Opt. Lett.*, vol. 35, no. 13, pp. 2118–2120, 2010.

[15] T. Holmgaard *et al.*, "Bend and splitting loss of dielectric-loaded surface plasmon-polariton waveguides," *Opt. Exp.*, vol. 16, no. 18, pp. 13585–13592, 2008.

[16] V. J. Sorger *et al.*, "Experimental demonstration of low-loss optical waveguiding at deep sub-wavelength scales," *Nature Commun.*, vol. 2, Art. no. 331, 2011.

[17] H.-S. Chu, E.-P. Li, P. Bai, and R. Hegde, "Optical performance of single-mode hybrid dielectric-loaded plasmonic waveguide-based components," *Appl. Phys. Lett.*, vol. 96, 2010, Art. no. 221103.

[18] A. V. Krasavin and A. V. Zayats, "Guiding light at the nanoscale: numerical optimization of ultrasubwavelength metallic wire plasmonic waveguides," *Opt. Lett.*, vol. 36, no. 16, pp. 3127–3129, 2011.

[19] T. R. Buckley and P. Berini, "Figures of merit for 2D surface plasmon waveguides and application to metal stripes," *Opt. Exp.*, vol. 15, no. 19, pp. 12174–12182, 2007.

[20] R. F. Oulton, G. Bartal, D. F. P. Pile, and X. Zhang, "Confinement and propagation characteristics of subwavelength plasmonic modes," *New J. Phys.*, vol. 10, 2008, Art. no. 105018.

[21] A. V. Krasavin and A. V. Zayats, "Silicon-based plasmonic waveguides," *Opt. Exp.*, vol. 18, no. 11, pp. 11791–11799, 2010.

[22] A. V. Krasavin and A. V. Zayats, "Passive photonic elements based on dielectric-loaded surface plasmon polariton waveguides," *Appl. Phys. Lett*, vol. 90, 2007, Art. no. 211101.

[23] A. V. Krasavin and A. V. Zayats, "Three-dimensional numerical modeling of photonic integration with dielectric-loaded SPP waveguides," *Phys. Rev. B*, vol. 78, 2008, Art. no. 045425.

[24] M. Georgas, J. Orcutt, R. J. Ram, and V. Stojanović, "A monolithically-integrated optical receiver in standard 45-nm SOI," *IEEE J. Solid-State Circuits*, vol. 47, no. 7, pp. 1693–1602, 2012.

[25] S. J. Orfanidis, *Electromagnetic Waves and Antennas*. New Brunswick, NJ, USA: Rutgers Univ., 2008.

[26] D. Yu. Fedyanin, A. V. Krasavin, A. V. Arsenin, and A. V. Zayats, "Surface plasmon polariton amplification upon electrical injection in highly integrated plasmonic circuits," *Nano Lett.*, vol. 12, pp. 2459–2463, 2012.

[27] D. A. B. Miller, "Rationale and challenges for optical interconnects to electronic chips," *Proc. IEEE*, vol. 88, no. 6, pp. 728–749, 2000.

[28] S. Manipatruni, M. Lipson, and I. A. Young, "Device Scaling Considerations for Nanophotonic CMOS Global Interconnects," *IEEE J. Sel. Topics Quantum Electron.*, vol. 19, no. 2, 2013, Art. no. 8200109.

[29] E. D. Palik, ed., *Handbook of Optical Constants of Solids*. New York, NY, USA: Academic, 1998.

[30] C. P. T. McPolin *et al.*, "Integrated plasmonic circuitry on a vertical-cavity surface-emitting semiconductor laser platform," *Nature Commun.*, vol. 7, Art. no. 12409, 2016.

[31] D. Fedyanin, A. V. Krasavin, A. Arsenin, and A. Zayats, "Electrically pumped coherent surface plasmon polariton source integrated on a chip," in *Proc. 7th Int. Conf. Surface Plasmon Photon.*, 2015, Art. no. Mo-01-P-33.

[32] R. F. Oulton *et al.*, "Plasmon lasers at deep subwavelength scale," *Nature*, vol. 461, pp. 629–632, 2009.

[33] K. Liu, C. R. Ye, S. Khan, and V. J. Sorger, "Review and perspective on ultrafast wavelength-size electro-optic modulators," *Laser Photon. Rev.*, vol. 9, no. 2, pp. 172–194, 2015.

[34] A. Melikyan *et al.*, "High-speed plasmonic phase modulators," *Nature Photon.*, vol. 8, pp. 229–233, 2014.

[35] H. W. Lee *et al.*, "Nanoscale conducting oxide PlasMOStor," *Nano Lett.*, vol. 14, no. 11, pp. 6463–6468, 2014.

[36] C. Lin and A. S. Helmy, "Dynamically reconfigurable nanoscale modulators utilizing coupled hybrid plasmonics," *Sci. Rep.*, vol. 5, Art. no. 12313, 2015.

[37] D. A. B. Miller, "Energy consumption in optical modulators for interconnects," *Opt. Exp.*, vol. 20, pp. A293–A308, 2012.

[38] P. Dong *et al.*, "Low V_{pp}, ultralow-energy, compact, high-speed silicon electro-optic modulator," *Opt. Exp.*, vol. 17, no. 25, pp. 22484–22490, 2009.

[39] D. Feng *et al.*, "High speed GeSi electro-absorption modulator at 1550 nm wavelength on SOI waveguide," *Opt. Exp.*, vol. 20, no. 20, pp. 22224–22232, 2012.

[40] R. Ding *et al.*, "Demonstration of a low V_{π}L modulator with GHz bandwidth based on electro-optic polymer-clad silicon slot waveguides," *Opt. Exp.*, vol. 18, pp. 15618–15623, 2010.

[41] K. Yoshida, Y. Kanda, and S. Kohjiro, "A traveling-wave-type LiNbO optical modulator with superconducting electrodes," *IEEE Trans. Microw. Theory Tech.*, vol. 47, pp. 1201–1205, 1999.

[42] R. C. Alferness, S. K. Korotky, L. L. Buhl, and M. D. Divino, "High-speed low-loss low-drive-power travelling-wave optical modulator for $\lambda = 1.32$ μm," *Electron. Lett.*, vol. 20, pp. 354–355, 1984.

[43] V. E. Babicheva, I. V. Kulkova, R. Malureanu, K. Yvinf, and A. V. Lavrinenko, "Plasmonic modulator based on gain-assisted metal-semiconductor-metal waveguide," *Photon. Nano. Fund. Appl.*, vol. 10, pp. 389–399, 2012.

[44] C. Koos *et al.*, "All-optical high-speed signal processing with silicon-organic hybrid slot waveguides," *Nature Photon.*, vol. 3, pp. 216–219, 2009.

[45] A. D. Neira, G. A. Wurtz, P. Ginzburg, and A. V. Zayats, "Ultrafast all-optical modulation with hyperbolic metamaterial integrated in Si photonic circuitry," *Opt. Exp.*, vol. 22, no. 9, pp. 10987–10994, 2014.

[46] M. Hochberg *et al.*, "Terahertz all-optical modulation in a silicon-polymer hybrid system," *Nature Mater.*, vol. 5, pp. 703–709, 2006.

[47] G. A. Wurtz *et al.*, "Designed ultrafast optical nonlinearity in a plasmonic nanorod metamaterial enhanced by nonlocality," *Nature Nanotechnol.*, vol. 6, pp. 107–111, 2011.

[48] N. C. Harris *et al.*, "Efficient, compact and low loss thermo-optic phase shifter in silicon," *Opt. Exp.*, vol. 22, no. 9, pp. 10487–10493, 2014.

[49] J. Gosciniak, L. Markey, A. Dereux, and S. I. Bozhevolnyi, "Efficient thermo-optically controlled Mach-Zhender interferometers using dielectric-loaded plasmonic waveguides," *Opt. Exp.*, vol. 20, no. 15, pp. 16300–16309, 2012.

[50] B. S. Dennis *et al.*, "Compact nanomechanical plasmonic phase modulators," *Nature Photon.*, vol. 9, pp. 267–273, 2014.

[51] J.-Y, Ou, E. Plum, J. Zhang, and N. I. Zheludev, "Giant nonlinearity of an optically reconigurable plasmonic metamaterial," *Adv. Mater.*, vol. 28, pp. 729–733, 2016.

[52] A. S. Shalin, P. Ginzburg, P. A. Belov, Y. S. Kivshar, and A. V. Zayats, "Nano-opto-mechanical effects in plasmonic waveguides," *Laser Photon. Rev.*, vol. 8, no. 1, pp. 31–36, 2014.

[53] Y. Akihama and K. Hane, "Single and multiple optical switches that use freestanding silicon nanowire waveguide couplers," *Light Sci. Appl.*, vol. 1, 2012, Art. no. e12.

[54] V. E. Babicheva *et al.*, "Towards CMOS-compatible nanophotonics: Ultra-compact modulators using alternative plasmonic materials," *Opt. Exp.*, vol. 21, no. 22, pp. 27326–27337, 2013.

ABOUT THE AUTHORS

Alexey V. Krasavin received the B.Sc. (with honors) and M.Sc. (with honors) degrees from the Moscow Institute of Physics and Technology, Moscow, Russia and the Ph.D. degree in physics from the University of Southampton, Southampton, U.K.

In 2006, he joined Queen's University Belfast, Belfast, Northern Ireland, as a Postdoctoral Research Fellow. Since 2010, he has been with King's College London, London, U.K. His research interests include the active manipulation and amplification of plasmonic signals, nonlinear plasmonic-assisted effects, plasmonic-enhanced fluorescence, and optical metamaterials.

Anatoly V. Zayats received the Ph.D. degree in physics from the Moscow Institute of Physics and Technology, Moscow, Russia.

He is the head of the Experimental Biophysics and Nanotechnology Group, Department of Physics, King's College London, London, U.K. His current research interests are in the areas of nanophotonics and plasmonics, metamaterials, nonlinear optics, and spectroscopy.

Dr. Zayats is a holder of the Royal Society Wolfson Research Merit Award, and a Fellow of the Institute of Physics, the Optical Society of America, the International Society for Optics and Photonics (SPIE), and The Royal Society of Chemistry.